Talanta 126 (2014) 61–72

Contents lists available at ScienceDirect

Talanta

journal homepage: www.elsevier.com/locate/talanta

Design, fabrication and evaluation of intelligent sulfone-selective polybenzimidazole nanofibers

Adeniyi S. Ogunlaja [a], Carol du Sautoy [b], Nelson Torto [a], Zenixole R. Tshentu [c,*]

[a] Department of Chemistry, Rhodes University, P.O. Box 94, Grahamstown 6139, South Africa
[b] Analytical Technology, Sasol Technology (Pty) Limited, P.O. Box 1, Sasolburg 1947, South Africa
[c] Department of Chemistry, Nelson Mandela Metropolitan University, P.O. Box 77000, Port-Elizabeth 6031, South Africa

ARTICLE INFO

Article history:
Received 27 November 2013
Received in revised form
20 February 2014
Accepted 15 March 2014
Available online 27 March 2014

Keywords:
Molecularly imprinted polymers
Organosulfur compounds
Desulfurization
Polybenzimidazole
Nanofibers

ABSTRACT

Molecularly imprinted polybenzimidazole nanofibers fabricated for the adsorption of oxidized organosulfur compounds are presented. The imprinted polymers exhibited better selectivity for their target model sulfone-containing compounds with adsorption capacities of 28.5 ± 0.4 mg g^{-1}, 29.8 ± 2.2 mg g^{-1} and 20.1 ± 1.4 mg g^{-1} observed for benzothiophene sulfone (BTO_2), dibenzothiophene sulfone ($DBTO_2$) and 4,6-dimethyldibenzothiophene sulfone (4,6-$DMDBTO_2$) respectively. Molecular modeling based upon the density functional theory (DFT) indicated that hydrogen bond interactions may take place between sulfone oxygen groups with NH groups of the PBI. Further DFT also confirmed the feasibility of π–π interactions between the benzimidazole rings and the aromatic sulfone compounds. The adsorption mode followed the Freundlich (multi-layered) adsorption isotherm which indicated possible sulfone–sulfone interactions. A home-made pressurized hot water extraction (PHWE) system was employed for the extraction/desorption of sulfone compounds within imprinted nanofibers at 1 mL min^{-1}, 150 °C and 30 bar. PHWE used a green solvent (water) and achieved better extraction yields compared to the Soxhlet extraction process. The application of molecularly imprinted polybenzimidazole (PBI) nanofibers displayed excellent sulfur removal, with sulfur in fuel after adsorption falling below the determined limit of detection (LOD), which is 2.4 mg L^{-1} S, and with a sulfur adsorption capacity of 5.3 ± 0.4 mg g^{-1} observed for application in the fuel matrix.

1. Introduction

The challenge of fulfilling the world's growing transportation fuel energy needs is no longer simple since the vast reservoirs of crude oils are sour (high sulfur content), and the growing concern over operational and environmental issues has increased over years [1]. Desulfurization of fuels is one of the main processes used in petroleum refinery to reduce sulfur concentration so as to meet environmental protection sulfur standards of 10–15 mg L^{-1} in fuels [1,2]. The conventional hydrodesulfurisation (HDS) process currently employed to remove sulfur suffers limitations such as the inability to efficiently eliminate refractory organosulfur compounds specifically dibenzothiophenes and the alkyl substituted dibenzothiophenes. On this account, the oxidative desulfurization (ODS) technique was proposed as a complementary desulfurization step to HDS as it eliminates refractory organosulfur compounds in hydrotreated fuels [2]. The ODS technique involves the oxidation of sulfur compounds followed by the extraction of the oxidized sulfur products (sulfonated compounds) [2]. The extraction of sulfonated compounds from oxidized fuels using solvents such as acetonitrile and dimethylsulfoxides (DMSO) eliminates other important compounds with similar chemical properties, consequently resulting in fuel properties and compositions falling outside the required specifications. Hence, the need to develop smart polymer nanofiber-based adsorbents [molecularly imprinted polymers (MIPs)] with large surface area-to-volume ratio for the selective removal of sulfonated compounds in fuels [2].

Electrospinning is a well-established technique for the production of nanofibers with diameters from nano-to-micrometer scale which possess very large surface area-to-volume ratio and high porosity [3–4], through the application of high voltage on polymer solution. It is an ancient technique, which was first observed by Rayleigh in 1897 as reported by Zeleny [5]. Zeleny, in 1914, studied electrospraying of liquids and the process was further developed and patented by Formhals [6] in 1934. However, Taylor's work [7] on electrically driven jets laid the foundation for electrospinning, since the findings were able to explain most of the processes governing nanofibers production. Over years, several applications of electrospun nanofibers have been reported. Burger et al. [8] and

* Corresponding author. Tel.: +27 41 504 2074; fax: +27 41 504 4236.
E-mail addresses: zenixole.tshentu@nmmu.ac.za, z.tshentu@gmail.com (Z.R. Tshentu).

http://dx.doi.org/10.1016/j.talanta.2014.03.035
0039-9140/

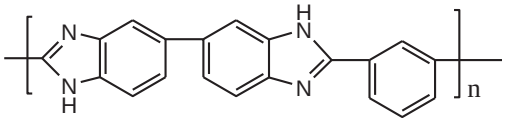

Fig. 1. Structure of polybenzimidazole (PBI).

Ramakrishna et al. [9] reported a very broad range of use of nanofibers, which includes adsorption [10,11], organ regeneration [12–15], electrospun scaffolds [16–21], fuel cells membrane [22], and catalyst supports [23–25].

Polybenzimidazole (PBI), a heterocyclic polymer with excellent chemical and thermal stability properties, was commercially developed by Celanese Corporation in 1983 for use as fire-retardant material and composite material reinforcement [26] due to the good molecular alignment [27,28]. Likewise, Sherrington et al. [29–31] as well as other researchers [32–35] have exploited the use of PBI as a support for a range of different metal-catalyzed reactions with great success. PBI comprises of repeating units of benzimidazole –NH groups (Fig. 1) which allows for hydrogen bonding interactions with polar compounds such as sulfones produced in the oxidation of organosulfur compounds in fuels [2,36–39].

Besides the possibility of PBI being a good adsorbent, desorption or extraction of isolated compounds from the adsorbent should generally be less problematic for material reusability. A safer desorption process that required the use of less hazardous solvents led to the evolution of green chemistry [40]. Green chemistry technology using subcritical fluids (pressurized hot water) for extraction and sample-preparation processes has proven to be a faster and more environmentally friendly process [40,41]. King et al. [42] reported that varying the temperature of water over a range of 25–250 °C under high pressure, changes its dielectric constant from 78 to less than 30, thereby attaining solvent polarities normally associated with polar organic solvents. Sulfone compounds display similar polar organic properties as pressurized hot water; thus, the latter will be a suitable and more economical candidate for sulfone extraction.

We describe for the first time, the fabrication of molecularly imprinted PBI nanofibers using benzothiophene sulfone (BTO_2), dibenzothiophene sulfone ($DBTO_2$), and 4,6-dimethyldibenzothiophene sulfone (4,6-$DMDBTO_2$) as templates. Absorption studies on model oxidized organosulfur compounds and oxidized hydrotreated diesel [36] were investigated in an attempt to produce ultra-pure fuels. This article also reports on the development of a simple pressurized hot water extraction method for desorption of the adsorbed sulfone compounds within the nanofibers matrix.

2. Experimental

2.1. Materials

Polybenzimidazole (PBI) was purchased from PBI performance products (Charlotte, USA) with intrinsic viscosity of 0.8 dL/g. Lithium bromide (LiBr) and Triton X-114 were purchased from Sigma Aldrich, Germany. Sulfur in diesel standards was purchased from Matheson Tri-Gas, Texas, USA. Sulfur standards produced by Matheson Tri-Gas have direct traceability to NIST SRM 2723a/SRM 2770 and are laboratory certified to ASTM D5453. *N*,*N*-dimethylacetamide (DMAc), acetonitrile (HPLC grade) and methanol (HPLC grade) were purchased from Merck, South Africa.

2.2. Sulfone compounds synthesis

Sulfone compounds (oxidized organosulfur compounds) were synthesized from the catalyzed oxidation of model organosulfur compounds such as benzothiophene, dibenzothiophene and 4,6-dimethyldibenzothiophene using poly[VO(allylSB-co-EGDMA)] and poly[VO(sal-AHBPD)] as oxidation catalysts [2,36].

2.2.1. Benzothiophene sulfone synthesis

0.15 g (0.0011 mol) benzothiophene (BT) was placed in a 25 mL round bottom flask containing 10 mL mixture of toluene/hexane (1:4) and 0.015 g (0.0135 mmol) of oxidation catalyst. The mixture was heated to 40 °C with continuous stirring at 500 rpm in an oil bath. An oxidant-to-substrate ratio of 6.8 was then added to the mixture. The oxidation reaction was allowed to proceed for 6 h under continuous stirring after the addition of *tert*-butylhydroperoxide. A white precipitate of benzothiophene sulfone (BTO_2) observed was collected through filtration and washed with hexane to remove unreacted benzothiophene. Yield=81%. ^{1}H NMR (δ, ppm in DMSO) δ 7.83 (d, J=7.2, 1H), 7.69 (t, J=7.4, 1H), 7.62 (t, J=9.1, 3H), 7.34 (d, J=6.8, 1H). *Anal.* Calcd. (found) for $C_8H_6O_2S$ (%): C, 57.81 (57.49); H, 3.64 (3.89); S 19.29 (19.02).

2.2.2. Dibenzothiophene sulfone synthesis

0.15 g, (0.00081 mol) dibenzothiophene (DBT) was dissolved in a 25 mL round bottom flask containing 10 mL mixture of toluene/hexane (1:4) and 0.015 g (0.0135 mmol) of oxidation catalyst. After which an oxidant-to-substrate ratio of 7.6 was added to the mixture and the oxidation reaction was allowed to proceed for 6 h under continuous stirring at 500 rpm at 40 °C. A white precipitate of dibenzothiophene sulfone ($DBTO_2$) was collected through filtration and washed with hexane to remove unreacted dibenzothiophene. Yield=98%. ^{1}H NMR (δ, ppm in DMSO): 8.22 (d, J=7.7, 2H), 8.00 (d, J=7.6, 2H), 7.82 (t, J=7.6, 2H), 7.67 (t, J=7.6, 2H). *Anal.* Calcd. (found) for $C_{12}H_{10}O_2S$ (%): C, 66.65 (66.02); H, 3.73 (4.04); S 14.83 (14.83).

2.2.3. 4,6-Dimethyldibenzothiophene sulfone synthesis

0.15 g (0.00071 mol) 4,6-dimethyldibenzothiophene (4,6-DMDBT) was dissolved in a 25 mL round bottom flask containing 10 mL mixture of toluene/hexane (1:4) and 0.015 g (0.0135 mmol) of oxidation catalyst. After which an oxidant-to-substrate ratio of 7.6 was added to the mixture and the reaction was allowed to proceed for 6 h under continuous stirring at 500 rpm at 40 °C. A white precipitate of 4,6-dimethyldibenzothiophene sulfone (4,6-$DMDBTO_2$) was collected through filtration and washed with hexane to remove unreacted dibenzothiophene. Yield=87%. ^{1}H NMR (δ, ppm in DMSO): 7.98 (d, J=7.6, 2H), 7.66 (t, 2H), 7.44 (d, J=7.5, 2H), 2.48 (s, 6H). *Anal.* Calcd. (found) for $C_{14}H_{12}O_2S$ (%): C 68.38 (68.38); H, 4.95 (5.25); S, 13.12 (12.83).

2.3. Instrumentation and methods

FT-IR spectra (4000–650 cm^{-1}) of PBI nanofibers were obtained on a Perkin Elmer 400 ATR-FT-IR spectrometer. Microanalysis was carried out using Elementar Analysen Systeme Vario® MICRO VI 6.2 GmbH. PBI nanofibers images and chemical characterization were carried out by using a TESCAN Vega TS 5136LM scanning electron microscopy (SEM) and an energy-dispersive spectroscopy (EDS) respectively. Before images were taken for SEM analysis, nanofibers were coated with a thin film of gold to prevent surface charging and also to protect the material surface from thermal damage by the electron beam. No surface coating was needed for EDS analysis. The BET surface area measurements of the nanofibers were performed by using a Micromeritics ASAP 2020 surface area analyzer. Prior to analysis, the nanofibers were degassed for 10 days at 50 °C. Nitrogen gas was employed as adsorption gas for the surface area measurements. High voltage power supply from Glassman High Voltage Inc., USA, was employed for the electrospinning of polymer solutions.

Adsorption studies on the model compound were monitored by employing an Agilent 7890A gas chromatograph fitted with a flame ionization detector (GC–FID). The GC conditions for the adsorption analyses was started with an oven temperature of 50 °C ramping to 80 °C for 2 min, and then increased to 300 °C at a rate of 20 °C min^{-1}, and finally held for 1 min. A gas chromatograph fitted with an atomic emission detector (GC–AED) was used to monitor the adsorption of the sulfur in diesel. The analyses on the Agilent G2350A, GC–AED, were started at an oven temperature of 45 °C ramped to 150 °C at 10 °C min^{-1} and then held for 5 min, and then increased to a final temperature of 320 °C at a rate of 20 °C min^{-1}, and was further maintained at 320 °C for 2 min. An AED detector for sulfur analysis was set at a wavelength of 181 nm (carbon analysis wavelength was 179 nm) with a transfer line temperature of 350 °C and block cavity temperature of 320 °C.

2.4. Electrospinning of polybenzimidazole solutions

PBI solution was prepared by dissolving 2.0 g of pristine PBI polymer in 10 mL *N*,*N*-dimethylacetamide containing 0.4 g (4 wt%) LiBr. The dissolution was carried-out under reflux condition in a nitrogen atmosphere for 4 h. The resulting viscous solution was cooled, and filtered to remove any particulates. LiBr (about 4% by weight) was employed for polymer dissolution as it increases solution electrospinability. To obtain imprinted PBI solution, 1 mL (0.01 M) acetonitrile solution of respective sulfone compounds containing 40 μL Triton X-114 (surfactant agent) was added to dissolved PBI polymer, after which the mixture was further stirred at 50 °C for 5 h to form a homogeneous blend. The polymer solution was transferred into a 25 mL syringe and electrospun by using the following optimized electrospinning conditions: a voltage between 20 and 25 kV at a flow-rate of 0.4 mL/h, with a distance between the needle tip and collector plate placed at 20 cm. The resulting nanofibers were subjected to an extensive washing process using a mixture of acetonitrile and methanol (1:1) *via* the Soxhlet extraction to remove residual solvent (DMAc) and entrapped template (sulfone compounds). The washed nanofibers were later dried overnight at an oven temperature of 60 °C.

2.5. Adsorption and desorption studies of model sulfone compounds

2.5.1. Adsorption studies of model sulfone compounds

Sulfone compounds adsorption studies were performed under batch conditions by weighing 50 mg of polybenzimidazole nanofibers into screw-capped vials containing 2 mL of 5 mM sulfone compounds {benzothiophene sulfone (BTO_2), dibenzothiophene sulfone ($DBTO_2$) and 4,6-dimethyldibenzothiophene sulfone (4,6-$DMDBTO_2$)}. The screw-capped vials containing sulfone compounds were left under mechanical agitation 150 rpm for 24 h after which the respective nanofibers were removed by filtration and the resultant solution analyzed by using GC-FID. Continuous flow adsorption process (Fig. 2) at a flow-rate of 1 mL h^{-1} employing similar nanofibers mass as the batch process was carried-out. Adsorption capacity, q_e (mg g^{-1}) was calculated from the following equation:

$$q_e = \frac{V(C_o - C_e)}{W} \quad (1)$$

where C_o, C_e, W and V are the initial concentration (mg L^{-1}), the equilibrium concentration (mg L^{-1}), the dry weight of nanofibers (g) and the solution volume (L) respectively. Conditioning of adsorbents was carried-out by pre-wetting adsorbents with solvents employed in dissolving the sulfone compounds.

2.5.2. Desorption/extraction procedure for the absorbed sulfone compounds

Molecularly imprinted nanofibers employed for adsorption were regenerated for reusability by the use of these following methods:

(i) Soxhlet extraction using a solvent mixture of acetonitrile and methanol (1:1). The Soxhlet extraction process was allowed to proceed for 12 h.
(ii) Pressurized hot water extraction (PHWE) system with desorption time of 40 min.

2.5.2.1. Pressurized hot water extraction. Water was employed as an alternative and cheaper green solvent for extraction/desorption of sulfone compounds under pressurized subcritical conditions. Water is termed "subcritical" when its temperature is between its boiling point (100 °C) and critical temperature (374.15 °C), in the presence of a pressure high enough to maintain it in the liquid state. In the subcritical region, water's dielectric constant is high thereby decreasing its polarity, thereby mimicking the properties of organic solvents [43].

A schematic image of pressurized hot water extractor is presented in Fig. 3. The system consists of an ion chromatography gradient pump (GS50, DIONEX), an oven (GC 5890A oven) and a stainless steel extraction vessel connected from the pump through the extraction sample holder to the collecting flask. The water temperature was set by means of a pre-heating coil inside the GC oven before entering the extraction vessel and also pressure build up was created through restrictions created on the metal tubing (Fig. 3). A cooling water bath (or ice bath) was used to cool the extract recovered, thus avoiding loss of products which may be caused by hot water. Optimization of the extraction process was carried out by varying oven temperatures (90, 120, 150, and 180 °C) at constant pressure (30 bar) and a flow rate of 1 mL min^{-1}. After each extraction process, the extraction vessel and metal tubing were flushed to eliminate any precipitated organic compound.

2.6. Molecular modeling for the proposed adsorption study

The density functional theory (DFT) for molecular modeling was employed to understand the mode of interactions between PBI and sulfone compounds [44,45]. Geometry optimisations and vibrational analyses of polybenzimidazole–sulfone adduct were performed using the Gaussian03 software. B3LYP functional was employed with a 6-31G(d) basis set [46]. The enthalpies of formation, Gibb's free energies and entropy of formation were calculated by using Eqs. (2) and (3) respectively [47].

$$\Delta\Delta H_{adduct} = \Delta H_{adduct} - (m\Delta H_{PBI} + t\Delta H_{sulfones}) \quad (2)$$

where m and t are the stoichiometric amounts of functional polymers and template molecules involved in complex formation.

$$\Delta\Delta G_{adduct} = \Delta\Delta H_{adduct} - T\Delta\Delta S_{adduct} \quad (3)$$

$\Delta\Delta G$, T and $\Delta\Delta S$ are the Gibbs free energy for the adduct formation, temperature (273 K) and entropy for adduct formation at standard conditions (*i.e.* 1 M concentration for solvents and 1 atm pressure) respectively.

3. Results and discussions

3.1. Characterization of fabricated imprinted and non-imprinted polybenzimidazole nanofibers

3.1.1. FT-IR and microanalysis of nanofibers

Brownish-yellow nanofibers were obtained after electrospinning and washing. From elemental analysis of imprinted

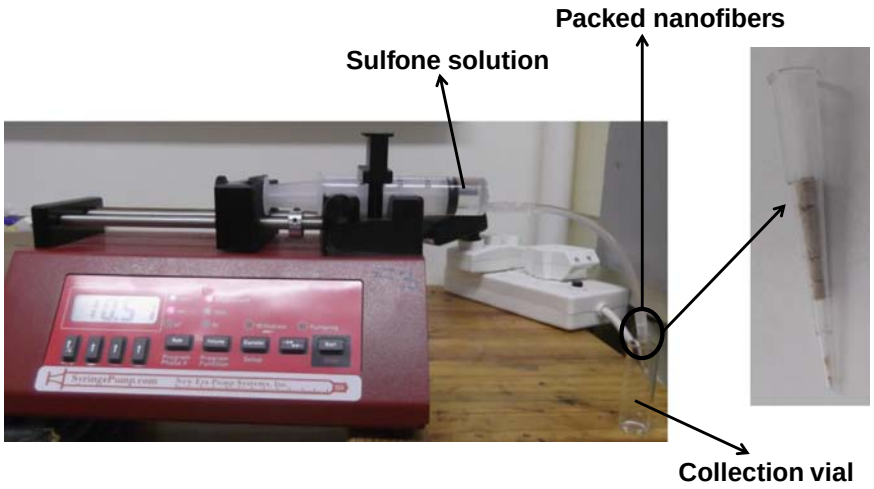

Fig. 2. The continuous flow setup used in this study. The filter tip compartment containing BTO_2-, $DBTO_2$- and 4,6-$DMDBTO_2$-imprinted nanofibers.

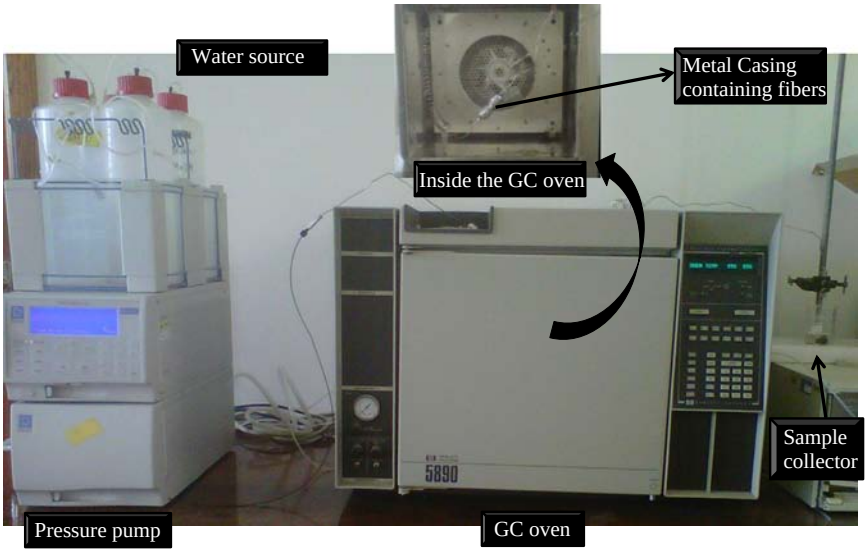

Fig. 3. A typical pressurized hot water extraction (PHWE) system.

nanofibers, C:N ratio remained constant as compared to the initial C:N ratio for PBI, hence indicating that polymers properties were retained. The FT-IR spectra of non-imprinted and imprinted nanofibers are presented in Fig. 4. *Anal.* Found for pristine PBI powder: C 71.28%, H 4.50%, N 16.55%, C:N ratio 4.31. IR (ν, cm^{-1}): 3403 (N–H), 1630, 1531 (C═N), 1446 (C═C). *Anal.* Found for PBI-nanofibers: C 61.92%, H 4.91%, N 14.09%, C:N ratio 4.39. IR (ν, cm^{-1}): 3411 (N–H), 1624, 1531 (C═N), 1439 (C═C). *Anal.* Found for PBI–BTO_2 nanofibers: C 58.06%, H 4.61%, N 13.00%, C:N ratio 4.47. IR (ν, cm^{-1}): 3430 (N–H), 1623, 1538 (C═N), 1438 (C═C). *Anal.* Found for PBI–$DBTO_2$ nanofibers: C 57.30%, H 4.94%, N 12.67%, C:N ratio 4.52. IR (ν, cm^{-1}): 3350 (N–H), 1630, 1530 (C═N), 1445 (C═C). *Anal.* Found for PBI–4,6-$DMDBTO_2$ nanofibers: C 59.54%, H 5.10%, N 13.75%, C:N ratio 4.33. IR (ν, cm^{-1}): 3388 (N–H), 1625, 1530 (C═N), 1440 (C═C).

3.1.2. Thermostability of nanofibers

Thermogravimetric analysis of non-imprinted PBI-nanofibers, PBI–BTO_2 nanofibers, PBI–$DBTO_2$ nanofibers and PBI–4,6-DMD-BTO_2 nanofibers was conducted under a nitrogen atmosphere (Fig. 5). The nanofibers (imprinted and non-imprinted) gave similar decomposition patterns with three distinct weight losses at 110 °C, between 220 and 400 °C and between 500 and 650 °C. The first two weight losses can be assigned to loosely bound solvent/water molecules, which occurred as a result of moisture absorption on fibers [48,49]. The decomposition of PBI nanofibers backbone only began to occur at a temperature of about 500 °C, hence confirming its high thermal stability [49,50]. For PBI nanofibers, a total of 19.3% weight loss was attributed to moisture and solvent molecule, while a further 20.7% weight loss occurred from 500 to 650 °C as a result of the breakdown in PBI polymer backbone. For BTO_2–PBI nanofibers, a total of 10.0% weight loss was attributed to moisture and solvent molecule, while a further 25.7% weight loss was due to the breakdown in polymer backbone from 500 to 650 °C. For $DBTO_2$–PBI nanofibers, a total of 8.1% weight loss was attributed to moisture and solvent molecule, a further 18.7% weight loss which occurred from 500 to 650 °C was as a result of a breakdown in the polymer backbone. For 4,6-$DMDBTO_2$–PBI nanofibers, a total of 9.7% weight loss was attributed to moisture and solvent molecule, while a further 7.3% weight loss occurred from 500 to 650 °C due to the partial collapse in the polymer backbone.

3.1.3. Scanning electron micrograph (SEM) images of nanofibers

SEM images of optimized imprinted and non-imprinted PBI nanofibers are presented in Fig. 6. The images showed some

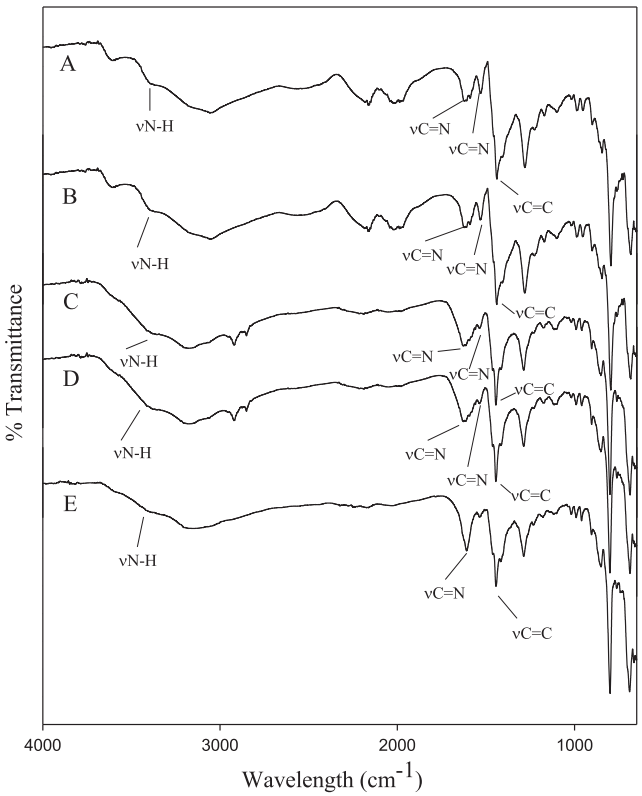

Fig. 4. FT-IR spectrum of (A) pristine PBI powder, (B) PBI-nanofibers, (C) PBI–BTO_2 nanofibers, (D) PBI–$DBTO_2$ nanofibers and (E) PBI–4,6-$DMDBTO_2$ nanofibers. PBI–BTO_2 nanofibers: benzothiophene sulfone imprinted polybenzimidazole nanofibers; PBI–$DBTO_2$ nanofibers: dibenzothiophene sulfone imprinted polybenzimidazole nanofibers; and PBI-4,6-$DMDBTO_2$ nanofibers: 4,6-dimethyldibenzothiophene sulfone imprinted polybenzimidazole nanofibers.

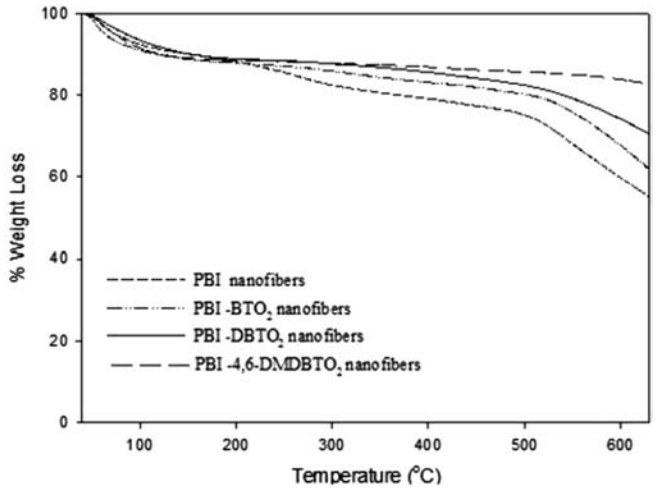

Fig. 5. TG profile for non-imprinted PBI-nanofibers, PBI–BTO_2 nanofibers, PBI–$DBTO_2$ nanofibers and PBI–4,6-$DMDBTO_2$ nanofibers.

surface morphological changes on imprinting the polybenzimidazole nanofibers. The nanofibers were generally observed to be in the diameter range of 150–330 nm. The images presented were collected after employing the Soxhlet extraction to remove the template. The absence of LiBr in the polymer solution resulted in the production of particles (from electrospraying) rather than fibers (from electrospinning) as shown in Fig. S1.

3.1.4. Energy dispersive spectroscopy (EDS) of nanofibers

The available functionalities (chemical composition) of imprinted and non-imprinted PBI nanofibers were evaluated by EDS as shown in Supplementary data (Fig. S2). The presence of trace amount of sulfur (S) within the imprinted nanofibers confirmed that imprinting took place, and further revealed that not all the sulfur containing molecules were removed after washing. The inability to completely remove all sulfur molecules (templates) is one of the major drawbacks in polymer imprinting. The bulk chemical composition of imprinted and non-imprinted nanofibers is presented in Table 1.

3.1.5. Surface area and porosity measurements of nanofibers

The BET adsorption and desorption isotherm is also presented in Supplementary data (Fig. S3). The porosity of various nanofibers increased as sulfone molecule size increased leading to a decrease in surface area. The molecule sizes of the sulfone compounds increased in the order $BTO_2 > DBTO_2 > 4,6\text{-}DMDBTO_2$, and were also evident in the pore size distribution values obtained for the various imprinted nanofibers. Surface area and porosity measurements of the various nanofibers are reported in Table 2.

3.2. Equilibrium swelling ratio of nanofibers

The thermodynamic compatibility of PBI nanofibers with solvents (acetonitrile and hexane) was explored by determining the swelling properties. Equilibrium swelling experiments were performed by weighing 50 mg PBI nanofibers and subsequently adding 5 mL of each selected solvent in 15 mL vials, the study was monitored at room temperature. The nanofibers were removed and weighed at specific time intervals by filtration through a Büchner funnel.

The equilibrium swelling ratio (ESR) was calculated as follows: $ESR = (W - W_o)/W_o$, where W_o and W are the initial and the final weight (mg) of nanofibers respectively with time [51]. From the results obtained, the nanofibers swelled more in acetonitrile as compared to hexane (Fig. S4), thus indicating that PBI nanofibers had poor affinity for a non-polar solvent such as hexane.

3.3. Adsorption results

3.3.1. Sulfone compounds adsorption selectivity of imprinted PBI nanofibers

Adsorption assays were carried out to evaluate the loading capacity and selectivity of imprinted PBI nanofibers. 50 mg of the imprinted adsorbents were added to vials and mixed with 2 mL solution mixture of organosulfur compounds, BTO_2, $DBTO_2$ and 4,6-$DMDBTO_2$ (5 mM). The corresponding adsorption assays were also carried out using non-imprinted adsorbents. The suspensions were left under mechanical agitation at 150 rpm for 24 h as described in the adsorption studies. Selectivity for sulfone compounds was confirmed as high adsorption capacities obtained for the sulfone compound solution which was in contact with its respective imprinted nanofibers, as compared to the non-imprinted and other imprinted nanofibers that displayed low adsorption capacities. Maximum adsorption observed for BTO_2, $DBTO_2$ and 4,6-$DMDBTO_2$ respectively was adsorption capacities of 28.5 ± 0.9 mg g^{-1}, 29.8 ± 1.2 mg g^{-1} and 20.1 ± 1.4 mg g^{-1} when imprinted PBI nanofibers were employed (Fig. 7). Desorption of sulfone compound was relatively high in both the imprinted and non-imprinted polymers. Adsorption of sulfone compounds unto nanofibers is said to be largely controlled by imprinting properties and physical factors (specific surface area and porosity, see Table 2) [52–54]. The observed phenomenon could be attributed to specific binding sites recognizable to their respective sulfone compounds owing to the size of sulfur compounds and the pore structure of adsorbent [55].

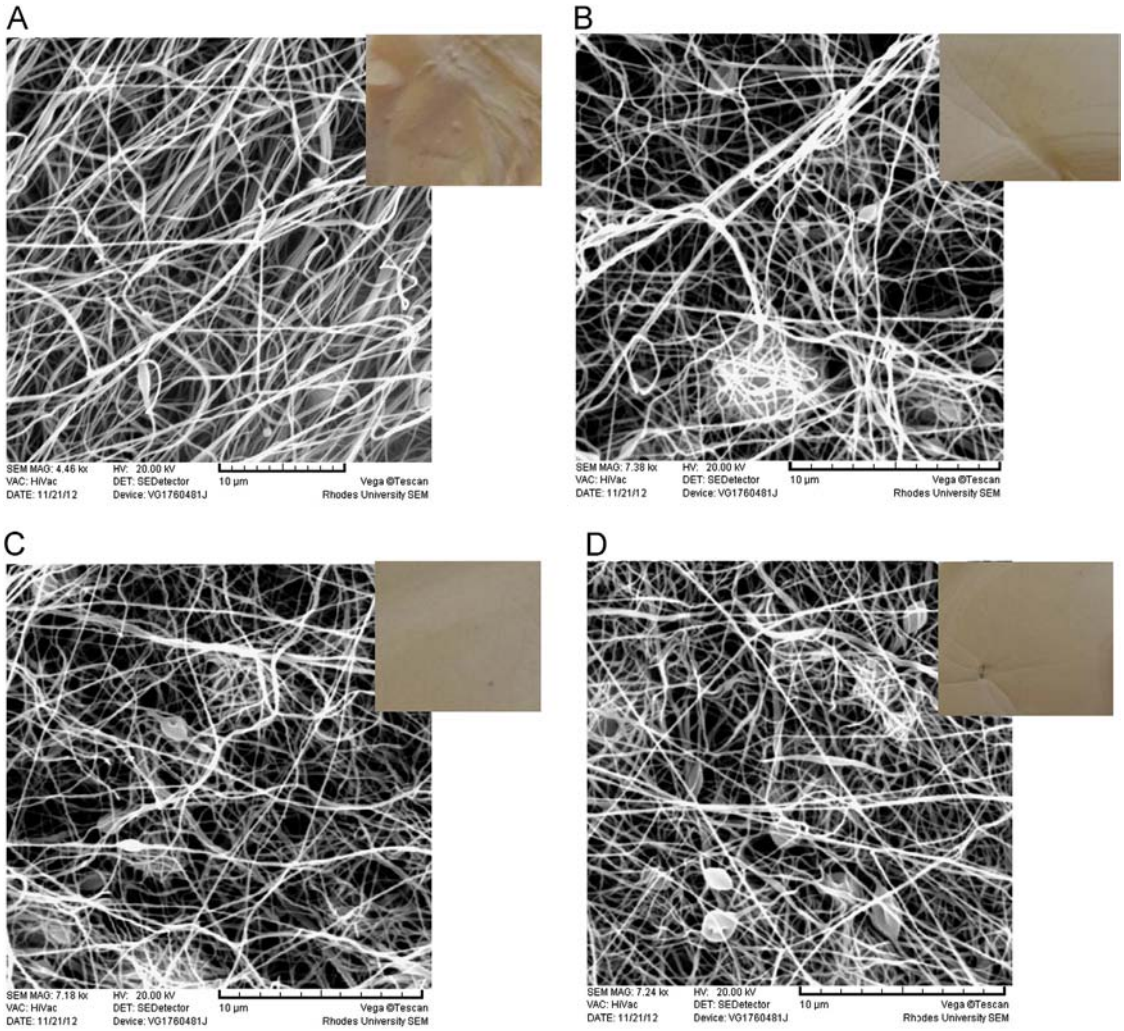

Fig. 6. Scanning electron microscopy (SEM) of (A) PBI-nanofibers, (B) PBI–BTO_2 nanofibers, (C) PBI–$DBTO_2$ nanofibers and (D) PBI–4,6-$DMDBTO_2$ nanofibers showing surface morphology.

Table 1
EDS chemical composition percentage abundance of nanofibers.

Elements	X-ray (keV)	Non-imprinted nanofibers	Imprinted nanofibers		
		NIP	BTO_2	$DBTO_2$	4,6-$DMDBTO_2$
Carbon (C)	0.277	73	75	73	74
Nitrogen (N)	0.392	18	16	18	16
Bromine (Br)	1.480	9	9	9	10
Sulfur (S)	2.307	–	0.1	0.3	0.3

Table 2
Surface area and porosity of PBI imprinted and non-imprinted nanofibers.

Adsorbent types	**Surface measurements**	
	Surface area (m^2/g)	**Pore size (Å)**
Non-imprinted (control)	35	104
BTO_2 imprinted	33	140
$DBTO_2$ imprinted	29	154
4,6-$DMDBTO_2$ imprinted	25	193

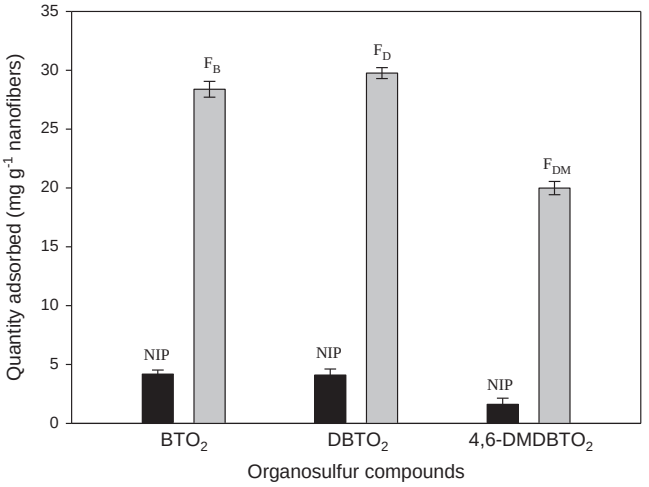

Fig. 7. Effect of selectivity on the adsorption of benzothiophene sulfone (BTO_2), dibenzothiophene sulfone ($DBTO_2$) and 4,6-dimethyldibenzothiophene sulfone (4,6-$DMDBTO_2$). NIF: non-imprinted nanofibers; F_B: benzothiophene sulfone imprinted nanofibers; F_D: dibenzothiophene sulfone imprinted nanofibers; F_{DM}: 4,6-dimethyldibenzothiophene sulfone imprinted nanofibers.

BTO_2-imprinted PBI nanofibers showed a high adsorption capacity of 28.5 ± 0.9 mg g^{-1} for BTO_2, while adsorption capacities for $DBTO_2$ and 4,6-$DMDBTO_2$ were 3.9 ± 0.6 mg g^{-1} and 2.6 ± 1.1 mg g^{-1} respectively on this material. $DBTO_2$-imprinted nanofibers' adsorption capacity for $DBTO_2$ was 29.8 ± 1.2 mg g^{-1}, while BTO_2 and 4,6-$DMDBTO_2$ adsorption capacities were 3.2 ± 0.3 mg g^{-1} and

2.5 ± 0.8 mg g^{-1} respectively. 4,6-DMDBTO$_2$-imprinted nanofibers gave an adsorption capacity of 20.1 ± 1.4 mg g^{-1} for 4,6-DMDBTO$_2$, while BTO$_2$ and DBTO$_2$ adsorption capacities were 4.1 ± 2.1 mg g^{-1} and 3.5 ± 1.2 mg g^{-1} respectively.

3.3.2. Sulfone binding selectivity coefficient

The selectivity coefficient (k) defined for imprinted adsorbents are given by Eq. (4). k is inversely related to a competitive affinity binding of molecule of interest competing with interfering molecule on the same binding site of the imprinted polymer. The higher the value of k, the better is the imprinting effect.

$$k = \frac{K_d \text{ (template molecule)}}{K_d \text{ (interfering molecule)}} \quad (4)$$

where $K_d = Q_e/C_e$ is the distribution coefficient of molecule between the nanofibers and the solution, and k is the selectivity coefficient. Two interfering molecules are been considered for each imprinted nanofibers.

The binding selectivity coefficient (k) values for BTO$_2$-imprinted nanofibers is 40.2, while DBTO$_2$-imprinted nanofibers is 12.9, and 4,6-DMDBTO$_2$-imprinted nanofibers is 10.9 respectively. From the obtained values, better template imprinting, which enhances adsorption selectivity, occurred as the template molecule decreases in size.

3.3.3. Sulfone compounds adsorption kinetics

Adsorption kinetics of imprinted nanofibers on respective sulfone compounds is presented in Fig. 8, with adsorption equilibrium as attained after 10 h. From the kinetic studies, sulfone compounds adsorption was initially fast due to the availability of surface adsorption, and thereafter adsorption rate slowed down as a result of surface saturation. From the adsorption curves, 4,6-DMDBTO$_2$ had the lowest adsorption capacity, due to the compounds steric hinderance nature, making the sulfone reactive center inaccessible. However, BTO$_2$ and DBTO$_2$ showed high adsorption, the quantity adsorbed increased in the order of DBTO$_2$ > BTO$_2$ > 4,6-DMDBTO$_2$.

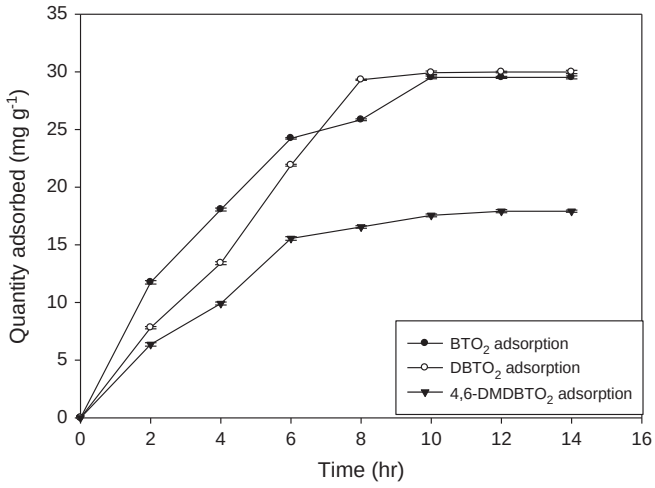

Fig. 8. Adsorption kinetics of the imprinted nanofibers on their respective sulfone compounds.

The kinetic mechanism that controlled the adsorption process was evaluated by the pseudo-first-order model (Eq. (5)) and the pseudo-second-order model (Eq. (6)). A batch adsorption process was employed to monitor the quantity of sulfone compound adsorbed with time.

$$\log(q_e - q_t) = \log q_e - \frac{K_1}{2.303}t \quad (5)$$

$$\frac{t}{q_e} = \frac{1}{q_e^2 K_2} + \frac{1}{q_e}t \quad (6)$$

where q_e and q_t (mg g^{-1}) are the amounts of sulfone compounds adsorbed on the nanofibers at equilibrium and time t, respectively. K_1 (h^{-1}) is the pseudo-first-order adsorption rate and was calculated by plotting $\log(q_e - q_t)$ versus t. K_2 (g mg^{-1} h^{-1}) is the adsorption rate constant of pseudo-second-order and was calculated from the slope and intercept of the plots t/q_t versus t (Fig. S5). From the two plots, pseudo-first-order adsorption rate was obeyed (Fig. S6). The pseudo-first order and pseudo-second order kinetic data are presented in Table 3.

3.3.4. Sulfone compounds adsorption Isotherms

Adsorption isotherms were also conducted under batch adsorption conditions using the same procedure described in Section 2.5.1. The Langmuir and Freundlich isothermal equations (Eqs. (7) and (8)) were employed to describe the equilibrium adsorption behavior.

$$\frac{C_e}{q_e} = \frac{C_e}{Q_m} + \frac{K_d}{Q_m} \quad (7)$$

$$\log q_e = \frac{1}{n}\log C_e + \log K \quad (8)$$

where q_e (mg g^{-1}) and C_e (mg g^{-1}) are the amount adsorbed at equilibrium time and the equilibrium concentration, (Q_m) is the theoretical maximum adsorption capacity at monolayer (mg g^{-1}) and K_d is the Langmuir constant (related to the affinity of adsorption sites) [56,57].

From the adsorption isotherms plots, the Freundlich adsorption data fitted better (larger correlation coefficient, R^2) as compared

Table 3
Kinetic data of pseudo-first-order and second order for the imprinted PBI nanofibers.

Adsorbents	Pseudo-first-order kinetics					
	BTO$_2$		DBTO$_2$		4,6-DMDBTO$_2$	
	k (h^{-1})	R^2	k (h^{-1})	R^2	k (h^{-1})	R^2
Nanofibers	1.512	0.9437	1.495	0.9336	1.312	0.9047
	Pseudo-second-order kinetics					
	BTO$_2$		DBTO$_2$		4,6-DMDBTO$_2$	
	k (g mg^{-1} h^{-1})	R^2	k (g mg^{-1} h^{-1})	R^2	k (g mg^{-1} h^{-1})	R^2
Nanofibers	5.614	0.0143	8.221	0.3281	8.620	0.3655

to the Langmuir parameters. The Freundlich constants, k and n indicating the adsorption capacity and the intensity respectively were determined from the linear plot of log q_e against log C_e (Fig. S7). From the study, the Freundlich constant, n, falls within the value range 1–10, thus indicating that adsorption on imprinted nanofibers was favorable [58]. The adsorption parameters for the Freundlich isotherm models are presented in Table 4.

3.3.5. PBI–sulfone interaction modeling studies

Three possible interaction sites for adduct formations between BTO_2, $DBTO_2$ and 4,6-$DMDBTO_2$ with polybenzimidazole (PBI) were modeled. These are (i) the compounds perpendicular (⊥) to PBI in *cis* position (site A), (ii) the compounds perpendicular (⊥) to PBI in *trans*/twisted position (site B) and (iii) the compounds parallel (∥) to PBI (site C). Thermodynamic parameters (especially negative $\Delta\Delta G$, Table 5) obtained for adducts formed in (i) compounds perpendicular (⊥) to PBI in *cis* position (site A) and (ii) compounds perpendicular (⊥) to PBI in *trans*/twisted position (site B) indicated that sulfone–PBI interactions were favorable as compared to (iii) sulfones parallel (∥) to PBI (site C) which present a positive $\Delta\Delta G$. The adduct formation occurred *via* π–π interaction and hydrogen bond formation through the interactions between sulfone oxygen groups with –NH groups of polybenzimidazole (Fig. 9). The order of adduct formation is given as $DBTO_2 > BTO_2 >$ 4,6-$DMDBTO_2$. This trend was also in conformation with the experimental adsorption results.

3.3.6. Reusability studies

Reusability studies of imprinted nanofibers were carried out by using the same adsorption studies described in the batch adsorption procedure. The rebinding adsorption–desorption capacities of the imprinted nanofibers are presented in Fig. 10. The imprinted PBI nanofibers presented a slight decrease in adsorption capacity upon the second cycle of usage as can be seen in Fig. 7 (first cycle) and 10 (second cycle), confirming the integrity of the imprinting effect as reported by Yonghui et al. [59]. From the second adsorption cycle, adsorption capacities of 24.2 ± 1.5 mg g^{-1}, 27.4 ± 1.2 mg g^{-1} and 17.8 ± 2.6 mg g^{-1} were observed for BTO_2, $DBTO_2$ and 4,6-$DMDBTO_2$ when respective imprinted PBI nanofibers were employed. The Soxhlet extraction using methanol/acetonitrile (1:1) was employed for desorbing the sulfone compounds from the nanofibers. Desorption was relatively high confirming the effective removal of adsorbed sulfone compounds from the polymer matrix (Fig. 10).

Table 4
Parameters of the Freundlich adsorption model for the imprinted PBI nanofibers.

Adsorbents	Freundlich parameters					
	BTO_2		$DBTO_2$		4,6-$DMDBTO_2$	
	n	R^2	n	R^2	n	R^2
Imprinted nanofibers	1.1197	0.9893	1.3613	0.9828	1.2470	0.9762

3.3.7. Desorption studies using a pressurized hot water extraction (PHWE)

Desorption/extraction yield increased as temperature increased up to 150 °C and afterwards began to decrease (Fig. 11). Sulfone compounds (oxidized organosulfur compounds) desorption yields from the respective imprinted PBI nanofibers for the first adsorption cycle was 98%, 85% and 94% for BTO_2, $DBTO_2$ and 4,6-$DMDBTO_2$, while the second cycle desorption yields were 95%, 89% and 97% for BTO_2, $DBTO_2$ and 4,6-$DMDBTO_2$. An extraction/desorption of 40–50 min was found to be optimal in desorbing the target compounds (sulfones), thus making the process faster than the Soxhlet extraction. PHWE did not have any negative effect on the reusability of the nanofibers as the cavity structural pores within the nanofibers were preserved. The pressure was reported to have no effect on the extraction efficiency as it was applied to establish the subcritical conditions of the solvent [60–63]. The major parameter that had a significant effect on extraction/desorption efficiency of sulfone compounds adsorbed with imprinted nanofibers was the applied temperature (Fig. 11).

3.4. Continuous flow adsorption studies

The continuous flow adsorption technique was employed for the adsorption of sulfone compounds. Breakthrough volumes were evaluated, as they represent the evolution of the concentration of a solution as a function of parameters such as contact time between liquid and solid phase, solvent concentration and temperature. 50 mg of imprinted nanofibers were packed into a cylindrical tube attached to the tip of a syringe containing 5 mL of 5 mM of the respective sulfone compound. The imprinted nanofibers were easily contained in the tube without leaving much space and the packing was tightened by conditioning the material with solvent at 1 mL h^{-1}. Adsorption progressed as respective sulfone compounds were pumped through the conditioned adsorbent at a flow-rate of 1 mL h^{-1}. From the adsorption curve, the maximum amount of sulfone compounds were retained only after 2 mL (2000 μL) of the solution has been dispensed (Fig. 12). The number of theoretical plates (N), the linear capacity of the column (n_s), the capacity factor of the solute (k) and percentage recovery (r) are calculated from the following equations [64,65] and presented in Table 5:

$$N = \frac{V_R}{\sigma_V^2}(V_R - \sigma_V)) \tag{9}$$

where $2\sigma_V = V_R - V_B$

$$K = \frac{V_R}{V_M} - 1 \tag{10}$$

$$n_s = V_M K C_o \tag{11}$$

$$r = \frac{n_s}{C_o V_o} \times 100\% \tag{12}$$

where V_o is the initial volume of the analyte (sulfone solution), V_B is the breakthrough volume, V_R is the retention volume, and V_M is the hold-up volume of the analyte (sulfone solution). From Table 6,

Table 5
DFT modeling studies on the formation adducts between benzothiophene sulfone, dibenzothiophene sulfone and 4,6-dimethydibenzothiophene with PBI ($\Delta\Delta H$, $\Delta\Delta G$ and $\Delta\Delta S$ adducts).

Complex	$\Delta\Delta H$ (kcal mol^{-1})			$\Delta\Delta G$ (kcal mol^{-1})			$\Delta\Delta S$ (cal mol^{-1})		
	BTO_2	$DBTO_2$	4,6-$DMDBTO_2$	BTO_2	$DBTO_2$	4,6-$DMDBTO_2$	BTO_2	$DBTO_2$	4,6-$DMDBTO_2$
Adduct ⊥ PBI plane, cis (site A)	−12.53	−13.26	−13.64	−2.27	−2.72	−2.45	−34.40	−35.37	−37.53
Adduct ⊥ PBI plane, twisted (site B)	−12.53	−13.27	−13.62	−2.27	−3.14	−2.01	−34.40	−34.00	−38.94
Adduct ∥ PBI plane (site C)	−9.41	−10.28	−7.69	0.73	0.63	3.46	−34.02	−36.57	−37.40

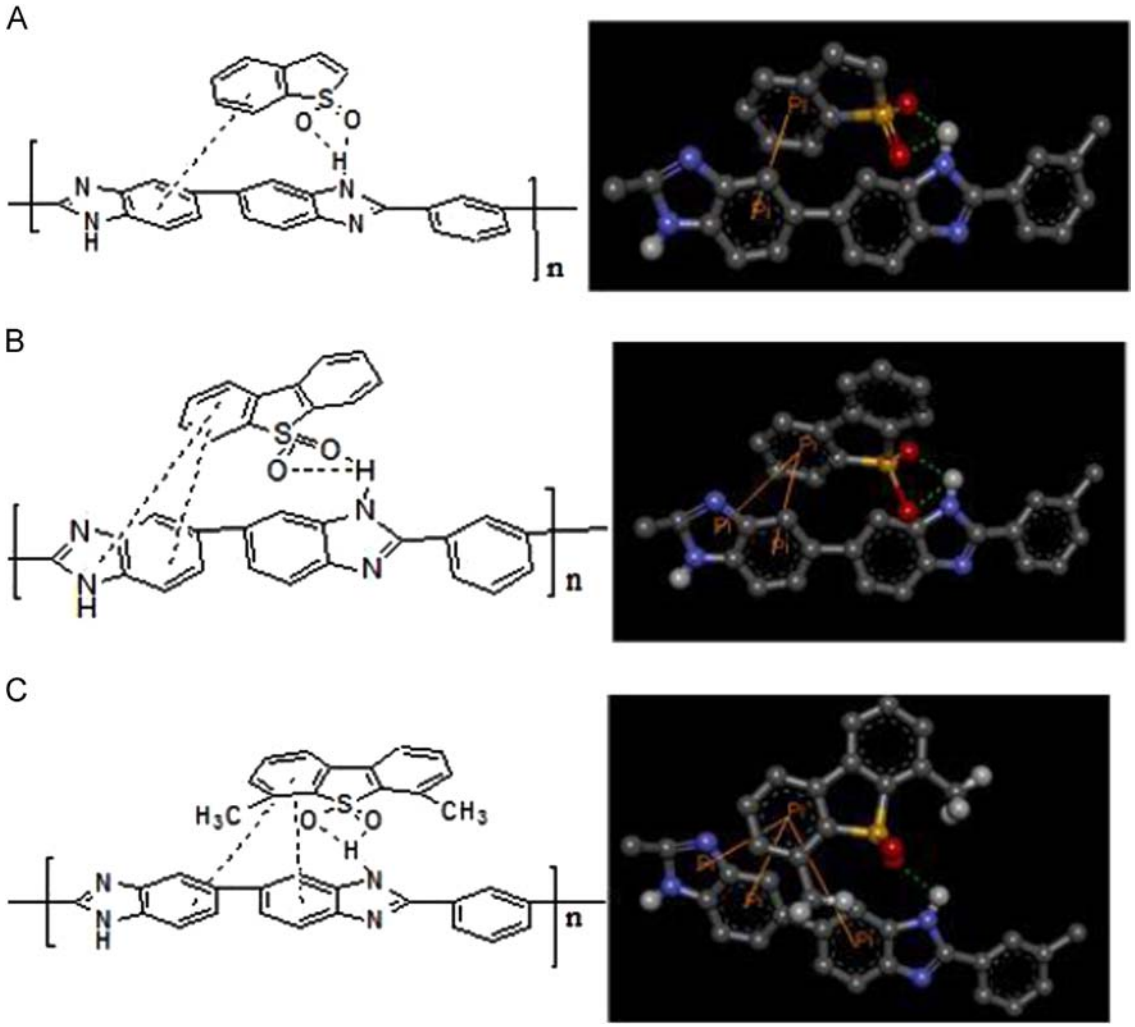

Fig. 9. Some modeling images employed for 1:1 adduct configuration of BTO_2 (A), $DBTO_2$ (B), and 4,6-$DMDBTO_2$ (C) with polybenzimidazole (PBI). Possibility of hydrogen bonding and π–π interactions are demonstrated.

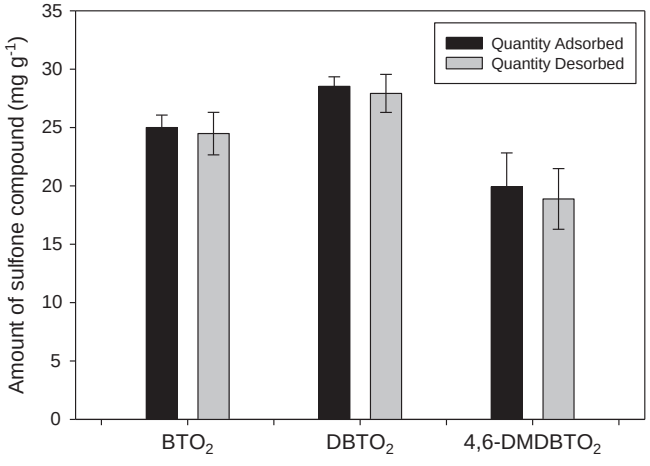

Fig. 10. Reusability of the imprinted nanofibers showing the adsorption/desorption capacities for the second cycle (cycle run was carried-out 3 times). Acetonitrile and methanol (1:1) were employed for desorption.

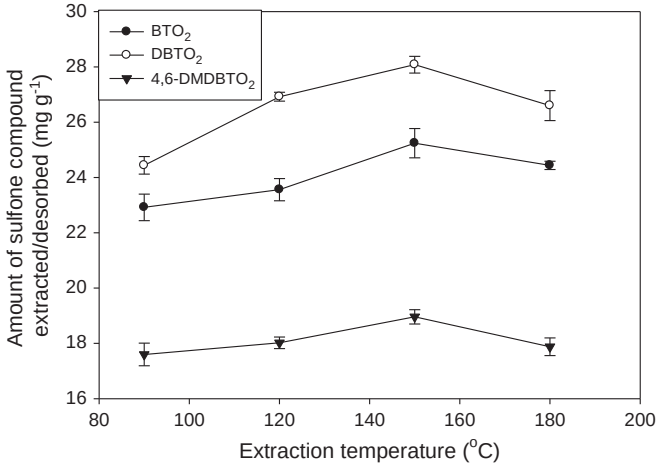

Fig. 11. Effects of temperature on the amount of sulfone compounds (analyte) extracted from imprinted PBI nanofibers by the PHWE method (first cycle). PHWE conditions: flow rate, 1 mL/min; time for extraction, 40–50 min; solvent, water ($n=3$).

a higher amount of $DBTO_2$ was recovered after continuous flow compared to BTO_2 and 4,6-$DMDBTO_2$. The breakthrough curves of the sulfone compounds solutions obtained are presented in Fig. 12. C_o is the initial concentration of the sulfone compounds and C_e is the eluted concentration of the sulfone compound.

3.5. Adsorption of mixture of model sulfone compounds (model oxidized fuel)

Adsorption studies using a solution containing a mixture of model compounds were carried out under a continuous flow

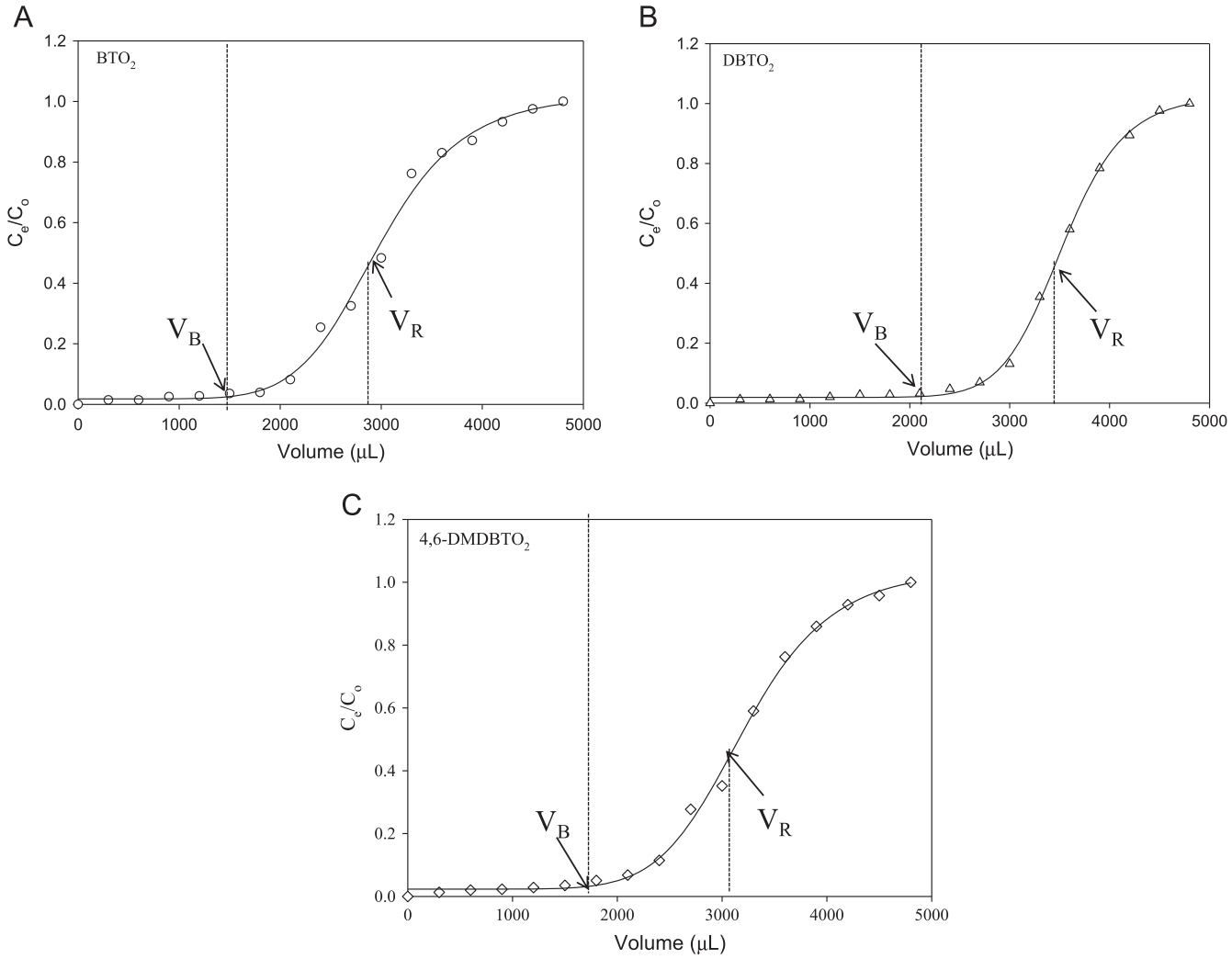

Fig. 12. Breakthrough curves of the various sulfone compounds (A) BTO_2 (B) $DBTO_2$ and (C) 4,6-$DMDBTO_2$ while using their various imprinted nanofibers.

Table 6
Influence of sulfone compounds upon adsorption on imprinted PBI nanofibers.

Sulfone compounds	V_B (mL)	V_R (mL)	V_M (mL)	N	k	n (mmol/g) $\times 10^{-2}$	r %
BTO_2	1.8	2.9	0.2	21.6	15.7	1.4	56.5
$DBTO_2$	2.1	3.5	0.2	20.9	12.9	1.6	64.5
4,6-$DMDBTO_2$	1.5	3.2	0.3	11.3	9.5	1.4	57.0

process and batch process by employing 150 mg of conditioned imprinted nanofibers (comprising of 50 mg BTO_2-imprinted nanofibers, 50 mg $DBTO_2$-imprinted nanofibers and 50 mg 4,6-$DMDBTO_2$-imprinted nanofibers).

The nanofibers were packed into a tube attached to a syringe containing 2 mL of a mixture of 830 mg L^{-1} BTO_2 (160 mg L^{-1} S), 1080 mg L^{-1} $DBTO_2$ (163 mg L^{-1} S) and 1230 mg L^{-1} 4,6-$DMDBTO_2$ (167 mg L^{-1} S); a similar mixture containing 150 mg of imprinted nanofibers was also contained in a screw-capped vial for batch adsorption process. A reduction in concentration of the sulfone compounds was observed after passing through the imprinted nanofibers (Fig. S8). For the continuous flow studies, BTO_2 was reduced to 37 mg L^{-1} (7.1 ± 1.4 mg L^{-1} S), $DBTO_2$ was reduced to 32 mg L^{-1} (4.7 ± 0.7 mg L^{-1} S) and 4,6-$DMDBTO_2$ was reduced to 22 mg L^{-1} (2.9 ± 0.2 mg L^{-1} S). In a batch adsorption process, BTO_2 was reduced to 151 mg L^{-1} (29.1 ± 4.6 mg L^{-1} S), $DBTO_2$ was reduced to 130 mg L^{-1} (19.3 ± 2.4 mg L^{-1} S) and 4,6-$DMDBTO_2$ was reduced to 85 mg L^{-1} (11.1 ± 0.9 mg L^{-1} S).

3.6. Adsorption and desorption of sulfone compounds in oxidized hydrotreated diesel

Oxidized hydrotreated diesel [36] containing sulfone compounds were desulfurized by using PBI imprinted nanofibers under continuous flow process gas chromatograph fitted with an atomic emission detector (GC–AED) which was used to monitor the adsorption of sulfur in the oxidized hydrotreated diesel. Prior to the sulfonated compound removal, the concentration of sulfur in the form of sulfonated compound in oxidized fuel was quantified, and a total sulfur content of 394 ± 4.2 mg L^{-1} S was observed. Some oxidized organosulfur compounds present in the oxidized fuel are provided in Table S1.

The linear plot of peak areas against standard sulfur concentrations presented in Fig. S9 was employed to determine the sensitivity (LOD and LOQ) of the GC–AED detection method [66,67]. The limit of detection (LOD) and limit of quantification (LOQ) were calculated from the respective following equations:

$$\mathrm{LOD} = \frac{3\mathrm{SD}}{S} \tag{13}$$

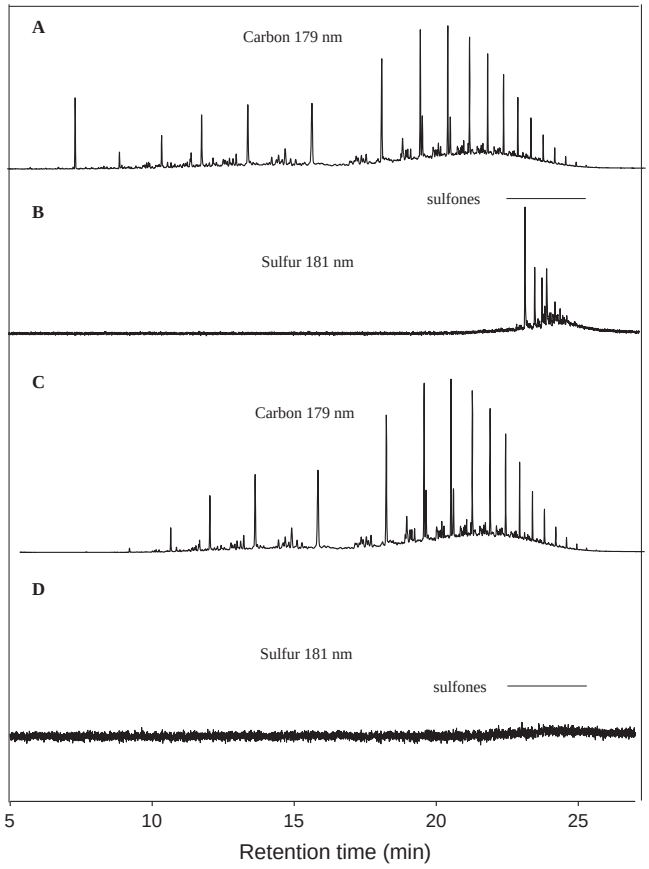

Fig. 13. GC–AED chromatograms of carbon (A) at 179 nm, and sulfur (B) at 181 nm in hydrotreated diesel after oxidation, and chromatograms of carbon (C) at 179 nm and sulfur (D) at 181 nm in oxidized hydrotreated diesel after using PBI-imprinted nanofibers as adsorbent.

$$\mathrm{LOQ} = \frac{10\mathrm{SD}}{S} \tag{14}$$

where SD is the standard deviation units, and S is the slope.

The limit of detection (LOD) and limit of quantification (LOQ) of the GC–AED analysis were found to be 2.4 μg S mL^{-1} and 7.6 μg S mL^{-1} respectively. The LOD represents the lowest concentration of sulfur in the sample which can be detected but not necessarily quantified as precise value while LOQ is the lowest concentration of sulfur in a sample which can be quantitatively determined with a high degree of confidence. The LOD and LOQ values obtained fall well below the 10 mg L^{-1} mandated sulfur limit in fuel [67]. 150 mg of conditioned imprinted PBI nanofibers (consisting of 50 mg BTO_2-imprinted nanofibers, 50 mg $DBTO_2$-imprinted nanofibers and 50 mg 4,6-$DMDBTO_2$-imprinted nanofibers) were applied for adsorption under continuous flow at a flow-rate of 1 mL h^{-1}. The sulfur left within the diesel after adsorption process could not be quantified as it is below the limit of detection (Fig. 13). The saturated sulfur adsorption capacity of the molecularly imprinted adsorbents was 5.3 ± 0.4 mg g^{-1}. Molecularly imprinted nanofibers displayed excellent adsorptive properties due to the imprinting effect, hydrogen bonding and π–π aromatic interactions.

Pressurized hot water extractions (PHWE) using the optimized extraction conditions (150 °C, 30 bar) were applied to desorb the adsorbed sulfone compounds on imprinted nanofibers; PHWE gave a higher desorption yield of 310 ± 2.9 mg L^{-1} S as compared to the Soxhlet extraction which gave an overall desorption yield of 216 ± 3.2 mg L^{-1} S (Fig. S10). The unavailability of CRMs for oxidized sulfur compounds in fuel, justify the lack of validation of the adsorption and desorption methods.

4. Conclusions

Imprinting of polybenzimidazole nanofibers enhanced their adsorption selectivity for individual sulfone compounds due to their specific binding nature and high adsorption capacities are reported. A better regression R^2 presented by the Freundlich isotherm confirmed multi-layer adsorption attributed to the interactions between PBI imprinted nanofibers and sulfone compounds, and possibly between sulfone molecules. Desorption of adsorbed sulfonated compounds from nanofibers using pressurized hot water extraction proved to be faster, environmentally friendly and gave better yields as compared to the Soxhlet extraction (methanol:acetonitrile, 1:1). Oxidized hydrotreated diesel containing 394 ± 4.2 mg L^{-1} S in the form of sulfonated compounds was removed below the limit of detection when imprinted PBI nanofibers were employed as absorbent under continuous flow adsorption conditions. Molecular modeling also confirmed that PBI nanofibers undergo hydrogen bond formation through the interactions between sulfone oxygen groups with –NH groups of the PBI and secondly *via* aromatic π–π stacking interactions between sulfone compounds and PBI. The high thermal stability and adsorption capacities of the imprinted polymers indicated its use as a potential adsorbent in the adsorption of sulfone compounds in the oxidative desulfurization (ODS) of fuels. However, validation of this method is still required once the standards containing oxidized sulfur compounds in fuel become available.

Appendix A. Supplementary material

Supplementary data associated with this article can be found in the online version at http://dx.doi.org/10.1016/j.talanta.2014.03.035.

References

[1] C. Song, U.T. Turaga, X. Ma, Encyclopedia of Chemical Processing, 651, http://dx.doi.org/10.1081/E-ECHP-120007732.
[2] A.S. Ogunlaja, S. Khene, E. Antunes, T. Nyokong, N. Torto, Z.R. Tshentu, Appl. Catal. A 462–463 (2013) 157–167.
[3] S. Ramakrishna, K. Fujihara, W.E. Teo, T. Yong, Z.W. Ma, R. Ramaseshan, Mater. Today 9 (2006) 40–50.
[4] W.E. Teo, S. Ramakrishna, Nanotechnology 17 (2006) 89–106.
[5] J. Zeleny, Phys. Rev. 3 (1914) 69–91.
[6] A. Formhals, Process and apparatus for preparing artificial threads, U.S. Patent no. 1. 975. 504, 1934.
[7] G.I. Taylor, Proc. R. Soc. Lond. Ser. A 313 (1969) 453–475.
[8] C. Burger, B.S. Hsiao, B. Chu, Annu. Rev. Mater. Res. 36 (2006) 333–368.
[9] Z.M. Huang, Z.Y. Zhang, M. Kotaki, S. Ramakrishna, Compos. Sci. Technol. 63 (2003) 2223–2253.
[10] H. Schreuder-Gibson, P. Gibson, K. Senecal, M. Sennett, J. Walker, W. Yeomans, P. Tsai, J. Adv. Mater. 34 (2002) 44–55.
[11] P. Gibson, H. Schreuder-Gibson, D. Rivin, Colloids Surf. A 187 (2001) 469–481.
[12] D.W. Hutmacher, W. Vanscheidt, Drugs Today 38 (2002) 113–133.
[13] Y.K. Luu, K. Kim, B.S. Hsiao, B. Chu, M. Hadjiargyrou, J. Controll. Release 89 (2003) 341–353.
[14] J.A. Matthews, G.E. Wnek, D.G. Simpson, G.L. Bowlin, Biomacromolecules 3 (2002) 232–238.
[15] R. Cancedda, B. Dozin, P. Giannoni, R. Quarto, Matrix Biol. 22 (2003) 81–91.
[16] S.R. Bhattarai, N. Bhattarai, H.K. Yi, P.H. Hwang, D.I. Cha, H.Y. Kim, Biomaterials 25 (2004) 2595–2602.
[17] J. Watanabe, T. Eriguchi, K. Ishihara, Biomacromolecules 3 (2002) 1375–1383.
[18] Y.Q. Wan, W.N. Chen, J. Yang, J.Z. Bei, S.G. Wang, Biomaterials 24 (2003) 2195–2203.
[19] W.J. Li, R. Tuli, C. Okafor, A. Derfoul, K.G. Danielson, D.J. Hall, R.S. Tuan, Biomaterials 26 (2005) 599–603.
[20] M. Shin, O. Ishii, T. Sueda, J.P. Vacanti, Biomaterials 25 (2004) 3717–3723.
[21] K.L. Elias, R.L. Price, T.J. Webster, Biomaterials 23 (2002) 3279–3287.
[22] L. Hsieh-Yu, L. Ying-Ling, J. Mater. Chem. A 1 (2013) 1171–1178.
[23] R.S. Walmsley, P. Hlangothi, C. Litwinski, N. Torto, T. Nyokong, Z.R. Tshentu, J. Appl. Polym. Sci. 127 (2012) 4719–4725.
[24] H.F. Jia, G.Y. Zhu, B. Vugrinovich, W. Kataphinan, D.H. Reneker, P. Wang, Biotechnol. Prog. 18 (2002) 1027–1032.
[25] R.S. Walmsley, A.S. Ogunlaja, M.J. Coombes, W. Chidawanyika, C. Litwinski, N. Torto, T. Nyokong, Z.R. Tshentu, J. Mater. Chem. 22 (2012) 5792–5800.

[26] P.K. Mallick, Fiber-reinforced compositesMarcel Dekker, New York, 1993.
[27] S.K. Kim, T.H. Kim, J.W. Jung, J.C. Lee, Polymer 50 (2009) 3495–3502.
[28] J.S. Kim, D.H. Reneker, Polym. Compos. 20 (1999) 124–131.
[29] M.M. Miller, D.C. Sherrington, J. Chem. Soc. Chem. Commun. (1994) 55–56.
[30] M.M. Miller, D.C. Sherrington, J. Catal. 152 (1995) 368–376.
[31] R. Mbeleck, K. Ambroziak, B. Saha, D.C. Sherrington, Stability and recycling of polymer-supported Mo(VI) alkene epoxidation catalysts, React. Funct. Polym. 67 (2007) 1448–1457.
[32] N.H. Li, J.M.J. Frechet, J. Chem. Soc. Chem. Commun. (1985) 1100–1101.
[33] R.M. Magdalene, E.G. Leelamani, N.M. Nanje-Gowda, J. Mol. Catal. A: Chem. 223 (2004) 17–20.
[34] A.A. D'Archivio, L. Galantini, A. Biffis, K. Jerabek, B. Corain, Chem. Eur. J. 6 (2000) 794–799.
[35] J.S. Kim, D.H. Reneker, Polym. Eng. Sci. 39 (1999) 849–854.
[36] A.S. Ogunlaja, R.S. Walmsley, C. du Sautoy, N. Torto, T. Nyokong, Z.R. Tshentu, Energy Fuels 27 (2013) 7714–7723.
[37] K. Ryu, J. Heo, I.K. Yoo, Biotechnol. Lett. 24 (2002) 143–146.
[38] B. Castro, M.J. Whitcombe, E.N. Vulfson, R. Vazquez-Duhalt, E. Barzana, Anal. Chim. Acta 435 (2001) 83–90.
[39] Y.Q. Xia, T.Y. Guo, M.D. Song, Z. Bang-hua, Z. Bao-long, React. Funct. Polym. 68 (2008) 63–69.
[40] P.T. Anastas, L.G. Heine, T.C. Williamson, Green EngineeringAmerican Chemical Society, Washington DC, 2001.
[41] J.W. King., in: E. Kiran, P.C. Debenedetti, C.J. Peters (Eds.), Supercritical Fluids – Fundamentals and Applications, Kluwer Academic, The Netherlands, Dordrecht, 2000, p. 457.
[42] J.W. King, C. R. Chim. 7 (2004) 647–659.
[43] A. Shotipruk, J. Kiatsongserm, P. Pavasant, M. Goto, M. Sasaki, Biotechnol. Prog. 20 (2004) 1872–1875.
[44] R.G. Parr, W. Yang, Density Functional Theory of Atoms and MoleculesOxford University Press, Oxford, 1989.
[45] R.M. Dreizler, E.K.U. Gross, Density Functional TheorySpringer, Berlin, 1990.
[46] M.J. Frisch, G.W. Trucks, H.B. Schlegel, G.E. Scuseria, M.A. Robb, J.R. Cheeseman, J.A. Montgomery Jr., T. Vreven, K.N. Kudin, J.C. Burant, J.M. Millam, S.S. Iyengar, J. Tomasi, V. Barone, B. Mennucci, M. Cossi, G. Scalmani, N. Rega, G. A. Petersson, H. Nakatsuji, M. Hada, M. Ehara, K. Toyota, R. Fukuda, J. Hasegawa, M. Ishida, T. Nakajima, Y. Honda, O. Kitao, H. Nakai, M. Klene, X. Li, J.E. Knox, H.P. Hratchian, J.B. Cross, V. Bakken, C. Adamo, J. Jaramillo, R. Gomperts, R.E. Stratmann, O. Yazyev, A.J. Austin, R. Cammi, C. Pomelli, J. W. Ochterski, P.Y. Ayala, K. Morokuma, G.A. Voth, P. Salvador, J.J. Dannenberg, V.G. Zakrzewski, S. Dapprich, A.D. Daniels, M.C. Strain, O. Farkas, D.K. Malick, A.D. Rabuck, K. Raghavachari, J.B. Foresman, J.V. Ortiz, Q. Cui, A.G. Baboul, S. Cliord, J. Cioslowski, B.B. Stefanov, G. Liu, A. Liashenko, P. Piskorz, I. Komaromi, R.L. Martin, D.J. Fox, T. Keith, M.A. Al-Laham, C.Y. Peng, A. Nanayakkara, M. Challacombe, P.M.W. Gill, B. Johnson, W. Chen, M. W. Wong, C. Gonzalez, J.A. Pople, Gaussian 03, Revision E.01Gaussian, Inc., Wallingford CT, 2004.
[47] W.J. Hehre, L.D. Burke, A.J. Shusterman, W.J.Pietro, Experiments in Computational Organic ChemistryWave function Inc., CA, USA, 1993.
[48] J. Jouanneau, R. Mercier, L. Gonon, G. Gebel, Macromolecules 40 (2007) 983–990.
[49] A. Sannigrahi, D. Arunbabu, R.M. Sankar, T. Jana, J. Phys. Chem. B 111 (2007) 12124–12132.
[50] J. Lobato, P. Canizares, M. Rodrigo, J. Linares, J. Aguilar, J. Membr. Sci. 306 (2007) 47–55.
[51] Z. Gao, J.S. Nahrup, J.E. Mark, A. Sakr, J. Appl. Polym. Sci. 90 (2003) 658–666.
[52] Z. Hu, M.P. Srinivasan, Y. Ni, Adv. Mater. 12 (2000) 62–65.
[53] C. Pelekani, V.L. Snoeyink, Carbon 38 (2000) 1423–1463.
[54] C. Pelekani, V.L. Snoeyink, Carbon 39 (2001) 25–37.
[55] A. Jorge, A. Mendez-Orozco, S. Le-Borgne, Chem. Eng. Process. 43 (2004) 1587–1595.
[56] R.J. Umpleby, S.C. Baxter, M. Bode, Anal. Chim. Acta 435 (2001) 35–42.
[57] Y.C. Wong, Y.S. Szeto, W.H. Cheung, Langmuir 19 (2003) 7888–7894.
[58] E.R. Treybal, Mass Transfer Operationsthird ed., McGraw Hill International Editions – Chemical Engineering Series, Singapore, 1981.
[59] C. Yonghui, Z. Lei, Y.Z.L. Hanjie, L. Hao, O. Pingkai, Appl. Biochem. Biotechnol. 160 (2010) 593–603.
[60] D.J. Miller, S.B. Hawthorne, A.M. Gizir, A.A. Clifford, J. Chem. Eng. Data 43 (1998) 1043–1047.
[61] A. Basile, M.M. Jimenez-Carmona, A.A. Clifford, J. Agric. Food Chem. 46 (1998) 5205–5209.
[62] E.S. Ong, S.M. Len, Anal. Chim. Acta 482 (2003) 81–89.
[63] B. Pongnaravane, M. Goto, M. Sasaki, T. Anekpankul, P. Pavasant, A. Shotipruk, J. Supercrit. Fluids 37 (2006) 390–396.
[64] A. Kubátová, D.J. Miller, B.S. Hawthorne, J. Chromatogr. A 923 (2001) 187–194.
[65] A. Gelencser, G. Kiss, Z. Krivacsy, Z. Varga-Puchony, J. Chromatogr. A 693 (1995) 217–225.
[66] D.A. Arinbruster, M.D. Tillman, L.M. Hubbs, Clin. Chem. 40 (1994) 1233–1238.
[67] H.M.N.H. Irving, H. Freiser, T.S. West, IUPAC Compendium of Analytical Nomenclature: Definitive RulesPergamon Press, Oxford, 1981.